AIP | Applied Physics Letters

Passive removal of immiscible spacers from segmented flows in a microfluidic probe

Xander F. van Kooten, Julien Autebert, and Govind V. Kaigala

Citation: Applied Physics Letters **106**, 074102 (2015); doi: 10.1063/1.4913202
View online: http://dx.doi.org/10.1063/1.4913202
View Table of Contents: http://scitation.aip.org/content/aip/journal/apl/106/7?ver=pdfcov
Published by the AIP Publishing

Passive removal of immiscible spacers from segmented flows in a microfluidic probe

Xander F. van Kooten, Julien Autebert, and Govind V. Kaigala
IBM Research-Zurich, Säumerstrasse 4, CH-8803 Rüschlikon, Switzerland

(Received 3 December 2014; accepted 4 February 2015; published online 18 February 2015)

Microfluidic probes (MFPs) are a class of non-contact, scanning microfluidic devices that hydrodynamically confine nanoliter volumes of a processing liquid on a surface immersed in another liquid. So far only chemical processes using a single processing liquid have been implemented using MFPs. In this letter, we present the design and implementation of a probe head that allows segmented two-phase flows to be used, which will enable different chemical species to be sequentially delivered to a surface in defined volumes and concentrations. Central to this probe head is a spacer-removal module comprising blocking pillars in the injection channel, a bypass and an orifice leading to the aspiration channel. We present a capillarity-based analytical model that provides insight into the functionality of the module based on geometrical parameters. In addition, we study the difference between two- and three-channel modules and predict a 30% reduction in fluctuation of the footprint of the confined liquid for the three-channel module. We show that such a module with a 15 μm pillar spacing, a 30 μm orifice width, and an oblique angle of 30° can remove immiscible spacers (Fluorinert FC-40) from an aqueous flow at a rate of up to 15 spacers per second while maintaining hydrodynamic confinement of processing liquid. [http://dx.doi.org/10.1063/1.4913202]

Techniques to localize (bio)chemicals on surfaces at the micrometer length scale enable numerous applications, such as local staining of tissue samples,[1] targeted stimulation of cells,[2,3] and patterning of biochemicals on surfaces.[4] To this end, we developed the microfluidic probe (MFP), a non-contact scanning probe technology that leverages hydrodynamic flow confinement (HFC).[5] HFC is achieved by injecting a processing liquid and aspirating it together with an immersion liquid to hydrodynamically confine picoliter volumes of the processing liquid at the apex of the probe (Figs. 1(a) and 1(b)).[6,7] Although the classical HFC has been demonstrated for single-step chemical processes, its potential can be further exploited by using it to perform multi-step assays. Implementation of such assays requires different chemical species to be sequentially delivered to a surface in defined volumes and concentrations.

To enable sequential chemistry, it is necessary to design a MFP head that can implement a broad range of multi-step processes while being flexible with respect to the number and properties of the sequenced liquids. Therefore, the sequence of liquids required must be generated outside the MFP head, where fast and reliable selector valves can be used. However, when using such valves, convective and diffusive dispersion[8] occur during the transport of liquids from the valve to the MFP head, leading to cross-contamination between sequential liquids. Kreutzer *et al.*[9] showed that flow segmentation by insertion of immiscible-phase (IP) spacers between slugs of a continuous-phase (CP) liquid can reduce dispersion of the slugs. Typically, the IP is an oil[10] or gas,[11] whereas the CP is aqueous. In this letter, we use oil as the immiscible phase.

The use of oil-in-water emulsions is not compatible with surface processing by HFC. The interfacial tension of the immiscible spacers in the continuous phase will cause the spacers to accumulate and coalesce at the apex of the head when they exit the injection channel. Furthermore, the accumulated IP can contaminate the surface and alter the flow of the processing liquid, preventing it from being hydrodynamically confined.

We designed, modeled, and tested a module for the removal of immiscible spacers from segmented flows in the MFP. This module relies on pinning and passive merging of an immiscible phase, a concept previously used by Niu *et al.*[12] for droplet dilution and by Günther *et al.*[11] for extraction of a continuous carrier phase. In this letter, we propose an analytical model describing the spacer-removal module, outline design considerations that determine its characteristics, and study the influence of the module on HFC.

To enable the use of segmented flows in combination with HFC, we developed a MFP head comprising a module that selectively removes the immiscible spacers from the flow by leveraging the difference in channel surface wetting of the CP and the IP. This approach was chosen for two reasons. First, it is compatible with common microfabrication techniques of microfluidic devices such as MFPs,[5] as the removal module can simply be drawn in CAD software without requiring any complex surface treatment[13–15] during fabrication. Second, the geometrical approach allows greater flexibility of microfluidic devices with respect to the used liquids.

To test the spacer-removal module (Fig. 1(c)), spacers were inserted at an on-chip T-junction and visualized in a serpentine channel (Fig. 1(b)). In the removal module (Fig. 2(a)), an aspiration channel (left) is connected to an injection channel (right) by a bypass. When an immiscible spacer arrives at the blocking pillars in the injection channel, partial

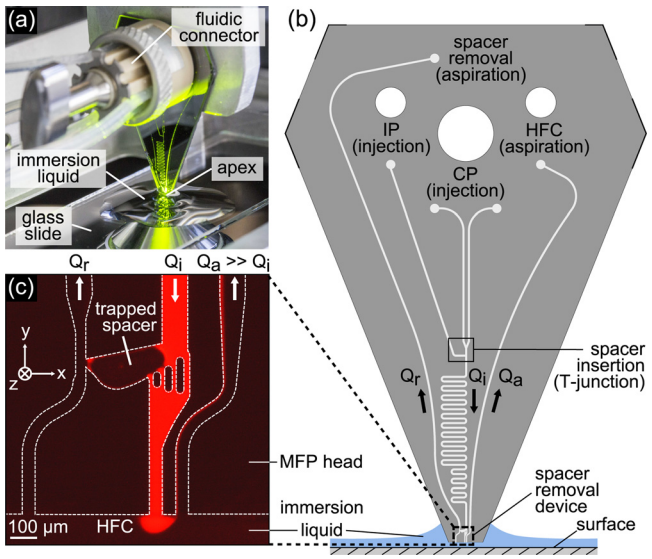

FIG. 1. The probe head with integrated spacer-removal module. (a) A vertically mounted MFP head processing a surface on an inverted microscope. (b) Schematic of the MFP with inlets for injection of CP and IP liquids. An on-chip spacer insertion junction and serpentine channel were used to test the spacer-removal module. (c) Micrograph of the immersed apex showing the spacer-removal module and hydrodynamic flow confinement (side view; no surface present). The spacer trapped in the bypass prevents the fluorescent CP (red) from flowing through the bypass; the CP continues towards the HFC.

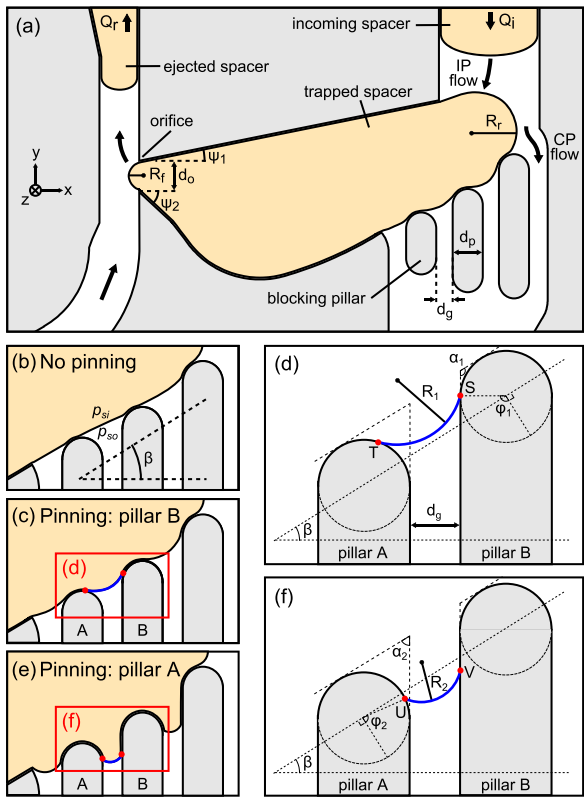

FIG. 2. Operating principle of the spacer-removal module. (a) An incoming immiscible spacer (top right) merges with a spacer that is trapped in the bypass, leading to ejection of IP into the removal channel (left). This sequence of events is influenced by pinning of the front interface at the orifice, and pinning of the side interface at the blocking pillars. The pinning behavior of the side interface is determined by the pillar spacing d_g and the oblique angle β. (b) For $p_{si} - p_{so} \ll P_{max,1}$, no pinning occurs at the side interface. (c) As $p_{si} - p_{so}$ approaches $P_{max,1}$, pinning occurs at pillar B. (d) For $P_{max,1} < p_{si} - p_{so} < P_{max,2}$, pinning occurs at pillar A. (e) Schematic close-up view of the interface (blue line) pinned at pillar B, having minimum curvature radius R_1. (f) Interface pinned at pillar A, with minimum curvature radius R_2.

pinning of its interface at the pillars causes it to be directed into the bypass, where it is then trapped due to a capillary force induced by the pinning of its front interface at the orifice.

When a subsequent incoming spacer reaches the blocking pillars, it merges with the spacer in the bypass and blocks the flow in the injection channel. The pressure increase resulting from this blockage causes a volume of IP to be ejected through the orifice into the removal channel (left in Fig. 2(a)) where it is sheared. As the module typically operates with a capillary number $Ca \approx 1$, the size of the ejected spacers can be modified by designing a constriction in the removal channel.[16] After the ejection of a fraction of the IP through the orifice, a trapped volume of IP prevents the continuous phase from flowing through the bypass. Subsequent incoming spacers will then be removed in a similar manner.

The pressure drop across the interface of the trapped spacer in the vicinity of the pillars ($p_{si} - p_{so}$ in Fig. 2(b)) is maximal when the flow in the injection channel is briefly blocked. This blockage occurs whenever an incoming spacer is merging with a trapped spacer. For the desired operation, the pressure in the injection channel must push the front interface of the spacer through the orifice before the side interface is pushed past the blocking pillars. By comparing the maximum pressure drop across the sections of the interface pinned at these two points (I and II, respectively, below) before the interface breaks, we determine how the module will remove spacers from the flow.

(I) Maximum pressure drop—across the front interface: The front interface of a trapped spacer is pinned at the orifice (Fig. 2(a)). The maximum pressure drop that this interface can withstand before breaking is given by the Laplace equation[17]

$$\Delta P_{f,max} = \gamma(1/\max\{R_{f,1}, R_{f,2}\} + 1/R_z), \qquad (1)$$

where γ is the interfacial tension of the oil-in-water emulsion, and R_f is the minimum curvature radius of this interface in the x, y plane, given by[12] $R_{f,i} = -d_o/(2\cos(\theta - \psi_i))$ $(i = 1, 2)$. Through similar geometrical reasoning, for the curvature radius in z-direction, we use[12] $R_z = -2\cos(\theta)/h$, where h is the channel height and θ is the contact angle. In the broadly applicable case where $\psi_1 \neq \psi_2$, both $R_{f,1}$ and $R_{f,2}$ must be evaluated as the larger of these two yields a lower maximum pressure drop $\Delta P_{f,max}$ and therefore determines the pressure drop at which the front interface breaks.

(II) Maximum pressure drop—at the blocking pillars: The side interface of a trapped spacer is in contact with the blocking pillars at all times. The development of a section of the side interface between pillars A and B consists of three stages.

(i) No pinning occurs when the pressure drop across the side interface is small compared with the maximum pressure drop that it can withstand before breaking (Fig. 2(b)).

(ii) As the pressure drop across the interface increases, the interface expands until the contact line at pillar B pins at point S (Figs. 2(c) and 2(d)). As $\theta \leq \pi$, the

interface is not affected by the straight left edge of pillar B below point S, and the interface will assume a symmetrical profile between S and T (Fig. 2(d)). We obtain an expression for the minimum curvature radius in the x, y plane by forcing the crossover angle (which provides a minimum curvature radius) $\varphi_1 = \alpha_1 = \pi/2 + \beta$ in the expression for pinning on cylindrical pillars[18]

$$R_{1,min}(\varphi_1) = \frac{d/2 - d_p \sin(\alpha_1)}{\sin(\theta - \alpha_1)}. \quad (2)$$

In Eq. (2), d is the pillar pitch in a rotated reference frame, given by $d = (d_g + d_p)/\cos(\beta)$. The maximum pressure drop that the interface can sustain before breaking is then $\Delta P_{1,max} = \gamma(1/R_{1,\min} + 1/R_z)$.

(iii) When the pressure drop across the side interface exceeds $\Delta P_{1,\max}$, the contact line on pillar A will proceed from T to U and the contact line on pillar B will slide downwards from S to V (Figs. 2(e) and 2(f)). A new pinning situation is established at U. The radius of the interface in the x, y plane in this position is derived geometrically

$$R_{2,\min}(\varphi_2) = \frac{1 - \cos\left(\beta + \varphi_2 - \frac{\pi}{2}\right) + d_g}{\cos\left(\frac{\beta}{2} + \frac{\varphi_2}{2} - \frac{\pi}{4}\right)\sin\left(\theta - \frac{\beta}{2} - \frac{\varphi_2}{2} - \frac{\pi}{4}\right)}, \quad (3)$$

where β is the oblique angle of the pillars, d_g is the spacing between pillars, and the crossover angle φ_2 was found numerically (Fig. 2(f)). We note that if the crossover angle does not satisfy $\varphi_2 \geq \alpha_2 = \pi/2 - \beta$, the point U will be situated on the transition from the circular to the straight edge of the pillar, and we must force $\varphi_2 = \alpha_2$ to find the minimum curvature radius. Laplace's law gives the maximum pressure drop that the interface can withstand in this position before breaking as $\Delta P_{2,\max} = \gamma(1/R_{2,\min} + 1/R_z)$.

The three stages described above can be translated into design requirements to obtain a functional module. At the side of the interface pinned at the pillars, the smaller of $R_{1,\min}$ and $R_{2,\min}$ will indicate whether the strongest pinning occurs in stage (ii) or (iii). We define a pressure ratio κ, which provides a comparison between the maximum pressure drop across the interface at the orifice and the blocking pillars. Equations (1)–(3) can be combined with Laplace's law to form the inequality

$$\kappa = \frac{1/(\max\{R_{f,1}, R_{f,2}\} + 1/R_z}{1/(\min\{R_{1,\min}, R_{2,\min}\} + 1/R_z} < 1. \quad (4)$$

For the front interface of the spacer to break at the orifice before the side interface breaks at the blocking pillars, κ must be smaller than one. Figure 3 shows the pressure ratio κ against the oblique angle of the pillars for various ratios of orifice width to pillar spacing (d_o/d_g).

According to Fig. 3, the design with $d_o/d_g = 2$ and $d_g = 15\,\mu$m satisfies $\kappa < 1$ for all oblique angles. Therefore, any angle can be chosen if the gap parameters d_o and d_g are kept constant. In doing so, we took into account the two additional consequences of changing the oblique angle β: (i) as β increases, the radius R_r of the rear interface decreases. A smaller radius of the rear interface of the trapped spacer leads to a higher pressure drop across that interface. This leads to more rapid merging with the front interface of an incoming spacer. (ii) The oblique pillars direct the incoming volume into the bypass more strongly as β increases, as pinning of the interface only occurs at the left edge of the pillars, while the section of the interface at the right edge is able to deform towards the bypass in the $-x$ direction. These two influences of β are related to the dynamics of spacer removal (interface propagation and merging) and are less easily quantified than the static (pinning) situation described by Laplace's law.

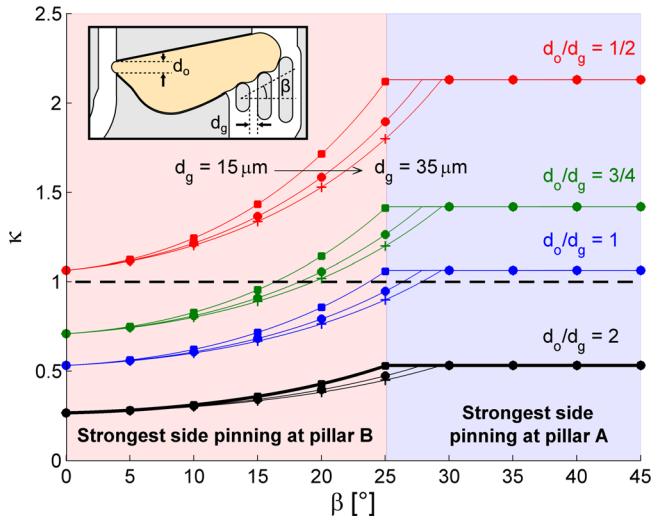

FIG. 3. Ratio between the maximum pressure drop across the front and side interface of the trapped spacer as a function of the oblique angle, for $\theta = 160°$. Common values $d_g = 15,\ 25,\ 35\,\mu$m (square, circle, cross) are shown. Correct operation of the module is achieved when $\kappa < 1$. For a given ratio of the orifice width (d_o) to pillar gap (d_g), the oblique angle determines whether the side interface is last pinned at pillar A (blue) or B (red) before break-up occurs at the orifice. The red and blue shadings are in the context of the bold black curve, describing a device that satisfies $\kappa < 1$ for all oblique angles.

Taking the design considerations above into account, we chose $\beta = 30°$ as a trade-off between a low pressure ratio κ, a small rear interface radius R_r and a unobstructed path along $-x$ for rapid merging of spacers.

Typically, the apex of the MFP head is about 20 μm from the surface, and the volume of confined liquid is on the order of 100 pl. A change in the volume of injected processing liquid from 100 pl to 120 pl then corresponds to a 10% increase of the radius of the footprint. The extent of the footprint variation, caused by hydrodynamic coupling between the removal module and the HFC, is important as it determines the accuracy and reproducibility of local surface processing. To study this coupling, we designed and compared two probe heads with different spacer-removal modules (Figs. 4(a) and 4(b)).

In a dual-aspiration module (Fig. 4(a)), $Q_{i,HFC} = Q_i - Q_{r,oil} = 0$ as the incoming spacer blocks the flow at the blocking pillar. This brief period without injection of processing liquid lasts for $\Delta t_{dual} = V_i/Q_i$. However, during this time, some processing liquid remains between the apex and the surface. If the time required to aspirate the remaining

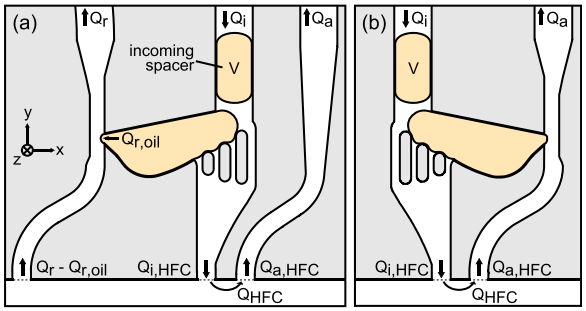

FIG. 4. Spacer-removal modules. (a) Module using three channels to implement the HFC and spacer removal. Stability of the HFC is increased by hydrodynamically decoupling the flows in the two aspiration channels. (b) Spacer removal can also be achieved using two channels.

volume of processing liquid exceeds Δt_{dual}, the hydrodynamic confinement persists. Therefore, by simply setting a higher arrival rate of spacers at the module, fluctuations in the footprint can be reduced.

In the two-channel module (Fig. 4(b)), a single aspiration inlet is used to form a HFC and to remove spacers coming from the removal module. In this case, an additional time $\Delta t_2 = V_o/Q_a$ is considered during which the flow of the immiscible phase from the bypass into the aspiration channel blocks the aspiration of continuous-phase processing and immersion liquid. Typically, the volume of incoming spacers is equal to the volume of ejected spacers.[12] Therefore, the time during which the area of the footprint is not constant is increased by $\Delta t_1 + \Delta t_2 - \Delta t_{dual} = 1 + Q_i/Q_a$ in the single-aspiration module as compared with the dual-aspiration module. Under standard operating conditions, where $Q_a \approx 3Q_i$, this corresponds to a total fluctuation time that is approximately 30% longer for the single-aspiration module.

We tested a spacer-removal module integrated into a MFP head using an emulsion of Fluorinert FC-40 in water containing 50 μM Rhodamine B for visualization. The fabrication of the silicon/glass MFP head is described elsewhere.[5] The MFP head had an on-chip T-junction for the insertion of FC-40 spacers upstream of the removal module. We observed a continuous HFC during removal (Fig. 5). It can be seen that the front interface at the orifice breaks before pinning occurs at pillar A, and that pinning of the interface at pillar B occurs with a crossover angle $\varphi_1 \approx 120°$. This indicates that the simple model based on the dimensionless parameter κ is sufficient to predict that pinning will first occur at the orifice, followed by pinning at pillars B and A.

We note that the model quantitatively describes only the static pinning behavior of the oil interface. Therefore, the model can be expected to accurately scale to different geometries (β, d_o, d_g). However, as discussed above, the model does not quantitatively describe the two dynamic influences on the removal characteristics of the spacer-removal module. The dynamic influences are independent of d_o and d_g but contribute to the removal characteristics more strongly as the oblique angle increases. This contribution is convenient when designing a functional device, as dynamic influences will lower the apparent pressure ratio κ. Correspondingly, our quantitative model of the static influences is expected to more accurately describe module geometries with low oblique angles than geometries with high angles ($\beta > 45°$).

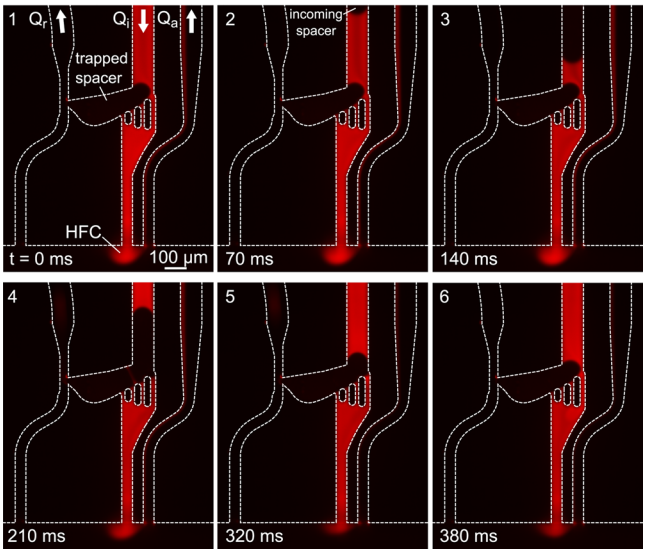

FIG. 5. Time sequence of colored CCD images showing the operation of a module with $\beta = 30°$, $d_o/d_g = 2$, and $d_g = 15\,\mu$m. An incoming spacer merges with the trapped spacer, leading to injection of oil into the left aspiration channel while maintaining a HFC (Rhodamine B fluorescence of continuous phase). Flow parameters are $Q_i = 1\,\mu$l/min, $Q_a = -10\,\mu$l/min, and $Q_r = -7\,\mu$l/min.

During typical experiments lasting tens of minutes, no injection of spacers into the immersion liquid was observed. After the flow was initiated, the module showed a consistent, predictable behavior, removing all spacers, and adapting to changes in the flow rates up to an arrival rate of ~15 spacers per second.

We demonstrated that two-phase segmented flows can be used in a microfluidic probe while maintaining a stable confinement of processing liquid. Such segmented flows open the route for localized sequential chemistry by reducing dispersion. With this, one can envision highly efficient patterning of proteins on surfaces and multiplexed immunohistochemistry on tissue sections.

This work was supported by the European Research Council (ERC) Starting Grant, under the 7th Framework Program (Project No. 311122, BioProbe). We thank Julien Cors, Ute Drechsler, and Yuksel Temiz for their help in fabrication and Andrew deMello and Robert Wootton (ETH Zürich) for valuable discussions. Carlotta Guiducci (EPFL), Robert Lovchik, Emmanuel Delamarche, Bruno Michel, and Walter Riess are acknowledged for their continuous support.

[1]M. S. Kim, T. Kim, S.-Y. Kong, S. Kwon, C. Y. Bae, J. Choi, C. H. Kim, E. S. Lee, and J.-K. Park, "Breast cancer diagnosis using a microfluidic multiplexed immunohistochemistry platform," PLoS ONE **5**, e10441 (2010).
[2]D. Chen, W. Du, Y. Liu, W. Liu, A. Kuznetsov, F. E. Mendez, L. H. Philipson, and R. F. Ismagilov, "The chemistrode: A droplet-based microfluidic device for stimulation and recording with high temporal, spatial, and chemical resolution," Proc. Natl. Acad. Sci. **105**, 16843–16848 (2008).
[3]A. Ainla, G. D. M. Jeffries, R. Brune, O. Orwar, and A. Jesorka, "A multifunctional pipette," Lab Chip **12**, 1255 (2012).
[4]A. J. You, R. J. Jackman, G. M. Whitesides, and S. L. Schreiber, "A miniaturized arrayed assay format for detecting small molecule-protein interactions in cells," Chem. Biol. **4**, 969–975 (1997).
[5]G. V. Kaigala, R. D. Lovchik, U. Drechsler, and E. Delamarche, "A vertical microfluidic probe," Langmuir **27**, 5686–5693 (2011).

[6]D. Juncker, H. Schmid, and E. Delamarche, "Multipurpose microfluidic probe," Nat. Mater. **4**, 622–628 (2005).
[7]G. V. Kaigala, R. D. Lovchik, and E. Delamarche, "Microfluidics in the 'open space' for performing localized chemistry on biological interfaces," Angew. Chem., Int. Ed. **51**, 11224–11240 (2012).
[8]G. Taylor, "Dispersion of soluble matter in solvent flowing slowly through a tube," Proc. R. Soc. London, Ser. A **219**, 186–203 (1953).
[9]M. T. Kreutzer, A. Günther, and K. F. Jensen, "Sample dispersion for segmented flow in microchannels with rectangular cross section," Anal. Chem. **80**, 1558–1567 (2008).
[10]J. G. Kralj, H. R. Sahoo, and K. F. Jensen, "Integrated continuous microfluidic liquid–liquid extraction," Lab Chip **7**, 256–263 (2007).
[11]A. Günther, S. A. Khan, M. Thalmann, F. Trachsel, and K. F. Jensen, "Transport and reaction in microscale segmented gas–liquid flow," Lab Chip **4**, 278–286 (2004).
[12]X. Niu, F. Gielen, J. B. Edel, and A. J. deMello, "A microdroplet dilutor for high-throughput screening," Nat. Chem. **3**, 437–442 (2011).
[13]G. Takei, M. Nonogi, A. Hibara, T. Kitamori, and H.-B. Kim, "Tuning microchannel wettability and fabrication of multiple-step Laplace valves," Lab Chip **7**, 596–602 (2007).
[14]T. Zhang and T. Cui, "Tunable wetting properties of patterned silicon microchannels with varied surface free energy based on layer-by-layer nano self-assembly," J. Micromech. Microeng. **21**, 045015 (2011).
[15]M. Eichler, K. Nagel, P. Hennecke, and C.-P. Klages, "Area-selective microplasma treatment in microfluidic channels for novel fluid phase separators," Plasma Process. Polym. **9**, 1160–1167 (2012).
[16]C. N. Baroud, F. Gallaire, and R. Dangla, "Dynamics of microfluidic droplets," Lab Chip **10**, 2032–2045 (2010).
[17]P.-G. De Gennes, F. Brochard-Wyart, and D. Quéré, *Capillarity and Wetting Phenomena: Drops, Bubbles, Pearls, Waves* (Springer, 2002).
[18]J. Berthier, F. Loe-Mie, V.-M. Tran, S. Schoumacker, F. Mittler, G. Marchand, and N. Sarrut, "On the pinning of interfaces on micropillar edges," J. Colloid Interface Sci. **338**, 296–303 (2009).